J Paleolimnol (2011) 46:405–421
DOI 10.1007/s10933-009-9373-0

ORIGINAL PAPER

Geochemical processes in a Mediterranean Lake: a high-resolution study of the last 4,000 years in Zoñar Lake, southern Spain

Celia Martín-Puertas · Blas L. Valero-Garcés · M. Pilar Mata · Ana Moreno · Santiago Giralt · Francisca Martínez-Ruiz · Francisco Jiménez-Espejo

Received: 30 November 2008 / Accepted: 18 August 2009 / Published online: 17 September 2009

Abstract High-resolution geochemical analysis of a 6-m-long sediment core from Zoñar Lake, southern Spain, provides a detailed characterization of major changes in lake and watershed processes during the last 4,000 years. Geochemical variables were used as paleolimnological indicators and complement Zoñar Lakes's paleoenvironmental reconstruction based on sedimentological and biological proxies, which define periods of increasing allochthonous input to the lake and periods of dominant autochthonous sedimentation. Chemical ratios identify periods of endogenic carbonate formation (higher Ca/Al, Sr/Al and Ba/Al ratios), evaporite precipitation (higher S/Al, Sr/Al ratios), and anoxic conditions (higher Mo/Al, U/Th ratios and Eu anomaly). Higher productivity is marked by elevated organic carbon content and carbonate precipitation (Mg/Ca). Hydrological reconstruction for Zoñar Lake was based on sedimentological, mineralogical and biological proxies, and shows that lower lake levels are characterized by Sr-rich sediments (a brackish lake with aragonite) and S-rich sediments (a saline lake with gypsum), while higher lake levels are characterized by sediments enriched in elements associated with alumino-silicates (Al, K, Ti,

C. Martín-Puertas (✉) · M. P. Mata
Departamento de Ciencias de la Tierra, Universidad de Cádiz. CASEM, 11510 Cádiz, Spain
e-mail: celia.martin@uca.es

M. P. Mata
e-mail: pilar.mata@uca.es

B. L. Valero-Garcés · A. Moreno
Instituto Pirenaico de Ecología-CSIC, Apdo 202, 50080 Zaragoza, Spain

B. L. Valero-Garcés
e-mail: blas@ipe.csic.es

A. Moreno
e-mail: amoreno@ipe.csic.es

S. Giralt
Instituto de Ciencias de la Tierra "Jaume Almera"-CSIC, C/Lluís Solé i Sabarís s/n, 08028 Barcelona, Spain
e-mail: sgiralt@ija.csic.es

F. Martínez-Ruiz · F. Jiménez-Espejo
Instituto Andaluz de Ciencias de la Tierra-(CSIC-UGR), Granada, Spain

F. Martínez-Ruiz
e-mail: fmruiz@ugr.es

F. Jiménez-Espejo
e-mail: fjjspejo@ugra.es

F. Jiménez-Espejo
Institute of Biogeosciences. Japan Agency for Marine-Earth Science and Technology (JAMSTEC), Natsushima-cho 2-15, Yokosuka 237-0061, Japan

Fe, trace and rare earth elements), reflecting fresher conditions. Geochemical indicators also mark periods of higher detrital input to the lake related to human activity in the watershed: (1) during the Iberian Roman Humid Period (650 BC–AD 300), around the onset of the Little Ice Age (AD 1400), during the relatively drier Post-Roman and Middle Ages (AD 800–1400), and over the last 50 years, due to mechanized farming practices. Heavy metal enrichment in the sediments (Cu and Ni) suggests intensification of human activities during the Iberian Roman Period, and the use of fertilizers during the last 50 years.

Keywords Paleolimnology · Geochemistry · Environmental changes · Land use · Iberian peninsula · Late Holocene

Introduction

Lakes are subject to interacting external and internal forcings, such as climate, tectonic and geomorphologic activity, changes in regional vegetation, aquatic biota and human activities (Cohen 2003). Interactions among these factors are complex and each lake is unique, controlled to some extent by its geographic and geologic setting. The rapid response of lakes to external and internal forcings, along with relatively high sedimentation rates, can lead to the preservation of high-resolution geochemical signals of environmental change in the deposits that accumulate on the lake bottom (Battarbee 2000). Geochemical studies of lake sediments have been used to infer past redox conditions (Eusterhues et al. 2005), atmospheric pollution (Nriagu 1996; Renberg 1986; Yang et al. 2003; Yang and Rose 2005; Schettler and Romer 2006; Ruiz-Fernández et al. 2007), human impact (Selig et al. 2007), weathering regimes (Koinig et al. 2003), and climate changes (Giralt et al. 2008; Moreno et al. 2008; Tanaka et al. 2007). The study of rapid climate or environmental changes is dependent on the ability to obtain good, high-resolution geochemical data from lake sediments. Recent improvements in techniques such as X-ray fluorescence (XRF) core scanning enable rapid collection of high-resolution chemical data from core profiles (Cheburkin and Shotyk 1996; Boyle 2000; Koinig et al. 2003; Mayr et al. 2005). This data acquisition technique has been commonly used on marine cores (López-Martínez et al. 2006; Röhl et al. 2004), and has recently been applied to lake cores (Brown et al. 2007; Moreno et al. 2007; Kristen et al. 2007). Trace metals and rare earth elements (REE) have not been used commonly as paleoenvironmental indicators, however they show potential as proxy measures of pollution and human activity (Borrego et al. 2006; Marmolejo-Rodríguez et al. 2007), as well as early diagenesis in lake sediment records (Sholkovitz and Szymczak 2000; Tanaka et al. 2007; Kylander et al. 2007).

The aim of this study was to identify the geochemical signature of the main depositional processes in Mediterranean Zoñar Lake, southern Spain, during the last 4,000 years, using high-resolution geochemical archives that combine qualitative and quantitative data (i.e. XRF scanner, ICP, AA). This high-resolution geochemical study provides an opportunity to evaluate the potential of geochemistry as a paleoenvironmental proxy, and to identify anthropogenic and climate forcing through comparison with previous paleohydrological reconstructions based on sedimentological and biological proxies (Valero-Garcés et al. 2006; Martín-Puertas et al. 2008, 2009).

Study area

Zoñar Lake (37°29′00″N, 4°41′22″ W, 300 m a.s.l.) is located in the Guadalquivir River Basin, Córdoba Province, Spain. The bedrock in the area consists of Triassic (carbonates, mudstones, evaporites and ophites) and Miocene marine formations (IGME 1988) (Fig. 1a). The origin of the lake basin is related to karst activity along fault structures (Sánchez et al. 1992). Currently, the lake has a maximum water depth of 14 m, a surface area of 3.7 km^2, and a watershed area of 88 km^2. Three main springs feed the lake (Fig. 1b) and most lake water is lost to evaporation (1,760 mm $year^{-1}$) (Enadimsa 1989). The lake is monomictic (thermally stratified from May to September), saline (TDS 2.4 g l^{-1}), and alkaline (pH 7.1–8.4). Lake water ionic composition is dominated by Na^+, Cl^-, and SO_4^{2-}. The watershed is strongly affected by anthropogenic activities, particularly cultivation of olive trees since Iberian times (500 years BC) (Martín-Puertas et al. 2008). The area has a semi-humid, Mediterranean climate with a mean annual rainfall of 538 mm (range 300–1,100 mm from 1985 to 2000),

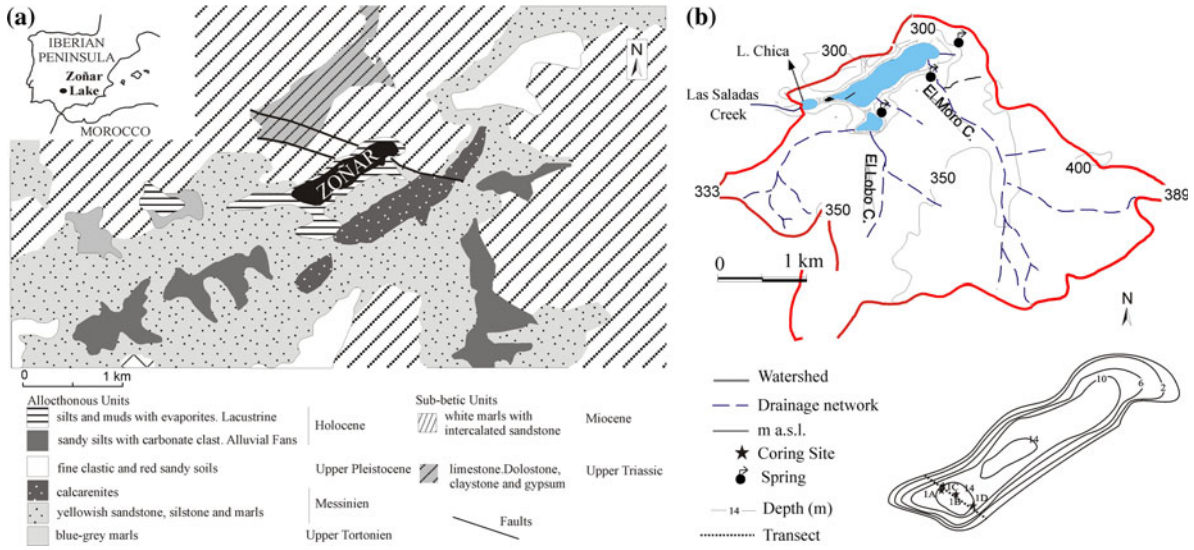

Fig. 1 **a** Geographic and geologic setting of Zoñar Lake (IGME 1988); **b** Zoñar Lake watershed and main springs (from NE to SW: Escobar, Zoñar and Eucaliptos). Modified from Valero-Garcés et al. (2006). Core sites are included (ZON04-1A, 1B, 1C and 1D)

with well-defined seasons characterized by wet, cool winters and warm, dry summers.

Materials and methods

In 2004, four Kullenberg cores were collected from the deepest area of Zoñar Lake along a 285-m transect, with a maximum distance between sites of 186 m (Fig. 1b). Core ZON 04-1B is 6 m long and spans the last 4,000 cal year according to the chronology described in Martín-Puertas et al. (2008) based on nine AMS ^{14}C dates, ^{137}Cs dating and varve counting. The sedimentological, mineralogical and biological composition of this sequence is described in detail elsewhere (Martín-Puertas et al. 2008, 2009). Geochemical data were obtained on sediment cores by three techniques: ICP-Mass spectrometry, Atomic Absorption spectrometry and XRF scanner. Trace and REE (Li, Rb, Cs, Be, Sr, Ba, Sc, V, Cr, Co, Ni, Cu, Zn, Ga, Y, Nb, Ta, Zr, Hf, Mo, Sn, Tl, Pb, U, Th, La, Ce, Pr, Nd, Sm, Eu, Gd, Tb, Dy, Ho, Er, Tm, Yb and Lu) were determined by Inductively Coupled Plasma-Mass Spectrometry (ICP-MS) with sample thickness of 1 cm each 10 cm, following HNO_3 + HF digestion. Measurements were made in triplicate by spectrometry (Perkin-Elmer Sciex Elan 5000, University of Granada) using Re and Rh as internal standards. Variation coefficients determined by the dissolution of 10 replicates of powdered samples were >3 and 8% for analyte concentrations of 50 and 5 μg g^{-1}, respectively (Bea 1996). Major elements (Fe, Mn, Al, Ca, Mg and K) were quantified using a Perkin Elmer model 5100 Atomic Absorption Spectrometer, model 5100 ZL ZEEMAN (University of Granada) with an analytic error of 2%. Major elements (Al, Si, S, K, Ca, Ti, Mn and Fe) were also measured at 5-mm resolution in massive units, and 2-mm resolution in laminated units, by an XRF core scanner (AVAATECH) at the University of Bremen, using 30-s count times, 10 kV X-ray voltage, and an X-ray current of 1,000 μA (massive units) and 500 μA (laminated units). Results from the XRF core scanner are expressed as element intensities in counts per second (cps). Elemental profiles of the major (Mg and Ca) and trace (Sr, Ba, Mo) elements were normalized to Al, since Al does not show fractionation and has very little ability to move during diagenesis (Calvert and Pedersen 1992; Piper and Perkins 2004). REE were normalized with respect to CI chondrite (Evensen et al. 1978; Boynton 1983). Eu/Eu* is calculated from $(Eu/(Sm*Gd))^{0.5}$. Statistical treatment of the data was performed using R software (R Development Core Team 2006). The dataset includes total organic carbon (TOC), total inorganic carbon (TIC) and total sulfur (TS), mineralogical composition (clay minerals, quartz, feldspar, calcite, aragonite, high-magnesium calcite (HMC), dolomite and gypsum) and magnetic susceptibility, described in

previous papers (Martín-Puertas et al. 2008, 2009), as well as new geochemical data (major, trace and REE and XRF scanner profiles). All variables were normalized with respect to their average and SD. Statistical significance tests are commonly used to evaluate the relationship between two variables, but some are affected by sample size, and their use is discouraged (Armstrong 2007). Instead, it is recommended that one report effect size, confidence intervals, replications/extensions and meta-analyses, because they are not affected by sample size (Nakagawa and Cuthill 2007). Pearson product-moment correlation (r) is one of the most widely used statistical variables, but many factors affect this correlation measure (Goodwin and Leech 2006). Therefore, we checked the effect sizes on quantitative geochemical data (major, trace and REE) employing Cohen's d as defined by Rosenthal and Rubin (1986), combined with confidence intervals (CIs), to obtain information on statistical significance that is not revealed by p values (Nakagawa and Cuthill 2007). The characterization of the effect sizes (small, medium and large) followed the definition of Cohen (1988).

Results

Statistical treatment

Table 1 summarizes the main sedimentological and geochemical properties of the sediment sequence.

Table 1 Sedimentary units description, geochemical stratigraphy and environmental deposits for Zoñar Lake from sedimentological study of core 1B in Martín-Puertas et al. (2008)

Units	Depth (cm)	Age	Sedimentary Description	Geochemical Stratigraphy	Environmental deposits
1	0–61	Modern-AD 1950	cm-bedded brown and gray massive calcite mud intercalated with 11-cm-thick laminated sediments	Predominance of Al, Si, K, Ti and Fe associated allochthonous trace elements as Rb, Sc, Zr or Zn. Cu enrichment (Cu/Al)	Littoral with alluvial influence
2	61–101	AD 1950–1800	Organic ooze laminated sediments[a] with authigenic calcite laminae	Mn enrichment (Mn/Fe) and high U, Mo and Sr	Benthic bacterial-algal mat
3	101–230	AD 1800–1200	10 cm-bedded gray and brown massive calcite mud	Predominance of Al, Si, K, Ti, Fe and trace elements associated and Ca enrichment. Abrupt Si peak at the middle of the unit corresponds to a quartz silty sand layer	Littoral with alluvial influence
4	230–289	AD 1200–600	cm-gypsum layer covered by calcite mud with high aragonite content and faintly laminated sediment[a] at the top	Upcore increase of Al, Si, K, Ti, Fe and trace elements associated. Enrichment in Li, Ba and Mg. Sharp peaks of U, Mo and Sr at the base	Brackish to saline lake
5	289–338	AD 600–300	cm-bedded gray and brown massive sediment	Decreasing trend Al, Si, K, Ti, Fe and trace elements associated. Increasing trend of Ca, Ba, Mg, and Sr	Littoral with alluvial influence
6	338–480	AD 300–550 BC	Fine, annually laminated sediments[a] (varves) with two 10-cm gypsum layers intercalated	Ca, Mg, Ba and Sr enrichment in well-preserved lamina. S and Sr predominance together with U and Mo at gypsum layers	Offshore lacustrine system
7	480–536	550–950 BC	Massive brownish sediments with aragonite and some pedogenic textures	Sr and Ba enrichments	Ephemeral brackish lake
8	536–600	950–2120 BC	Massive brown quartz and clay-rich sediment with pedogenic textures	Predominance of Al, Si, K, Ti, Fe and trace elements associated and Si enrichment at the upper part of the unit	Dry out to ephemeral lake

[a] Laminated sediments sequence in form of mm-layers of authigenic calcite, organic (diatoms and alga remains) and carbonate mud

Effect sizes (Pearson's r and Cohen's d) and confidence intervals (CI) for major, trace and REE were calculated to estimate statistical significance (Table 2). There is a large effect size ($r > 0.95$ and $d > 0.8$) between Cs, Cr, Zn, Ga, Y, Nb, Ta, Zr, Hf, Sn, Tl and Th, which allowed us to lump them as group I. Li is also related to group I ($5 > d > 2$ with 95% CI = 2–6). Fe, Al, K, Rb, Sc, Be, Co, also show a large effect size and statistical significance with group I, however these elements are related with other variables. Fe correlation is statistically significant with Mg, Al and Rb with Pb and Ca and Mg with Mo, U. To obtain a reliable approach and simplify the interpretation, but still capture most if its variance, multivariate analyses were applied.

The dataset includes major elements, trace elements, and REE (included in group I), and also bulk geochemistry (TOC, TIC and TS), magnetic susceptibility and mineralogy, collected at different sampling intervals. Trace elements determined by ICP had the lowest sampling resolution (10 cm), and the dataset contains 34 variables and 53 cases. The XRF dataset had higher resolution (5–2 mm) and it contained 1,699 cases. Comparison of the principal component analyses of the XRF data at 5–2 mm resolution (1,699 cases) and 10 cm (53 cases) shows that the combination of the variables is similar in both (Table 3), and, consequently, there is no information loss if we reduce the number of cases.

Redundancy Analysis (RDA) was carried out to investigate the relationship between mineralogical and geochemical composition of the sediments. An additional fuzzy sampling (25 samples of the dataset, not shown) was carried out and PCA was applied and compared with RDA using the 53 cases (Fig. 2). The results were similar. In the PCA, vectors of Be, V, Sc, Li, Ni, Co and Pb are in the third quadrant, showing similar statistical behavior. These elements have been grouped and called group II. Ca, Mn, Ba and Cu scores vary when geochemical elements are constrained to mineral composition (RDA), indicating that these elements could have more than one origin and they should be interpreted separately. The RDA biplot (Fig. 2) shows elements associated with mineral composition that define three sediment components:

1. *Allochthonous component* characterized by high values of Al, Si, K, Fe, Ti, Rb, Cu and groups I and II. This component is characterized by the

Table 2 Effect size (Pearson's r) among major and trace elements and REE measured for Zoñar Lake samples

	Fe	Mn	Al	Ca	Mg	K	Li	Rb	Cs	Be	Sr	Ba	Sc	V	Cr	Co	Ni	Cu	Zn	Ga	Y	Nb	Ta	Zr	Hf	Mo	Sn	Tl	Pb	U	Th	REE
Fe	1.00																														
Mn	0.13	1.00																													
Al	0.83	-0.15	1.00																												
Ca	-0.61	0.16	-0.63	1.00																											
Mg	**0.02**	0.40	-0.07	0.21	1.00																										
K	**0.81**	0.02	**0.76**	-0.57	0.15	1.00																									
Li	0.54	0.30	**0.38**	-0.22	0.76	0.60	1.00																								
Rb	0.95	-0.03	0.91	-0.63	-0.13	0.84	0.44	1.00																							
Cs	**0.95**	-0.04	**0.88**	-0.61	-0.14	**0.81**	**0.**	**0.99**	1.00																						
Be	**0.87**	-0.01	**0.77**	-0.51	-0.18	**0.69**	**0.36**	0.90	**0.91**	1.00																					
Sr	-0.73	0.15	-0.59	0.65	0.36	-0.58	-0.13	-0.72	-0.74	-0.66	1.00																				
Ba	-0.04	0.41	0.03	0.10	0.41	0.06	0.28	-0.05	-0.10	-0.08	0.21	1.00																			
Sc	**0.83**	0.03	**0.76**	-0.35	-0.23	0.,50	0.24	**0.84**	0.84	0.85	-0.59	-0.11	1.00																		
V	0.81	0.17	0.69	-0.54	0.17	0.56	0.51	0.72	0.74	0.62	-0.49	0.10	0.66	1.00																	
Cr	0.94	-0.02	0.88	-0.58	-0.19	0.74	0.37	**0.98**	**0.98**	0.92	-0.73	-0.08	**0.91**	**0.75**	1.00																
Co	**0.91**	0.27	**0.79**	-0.50	0.03	0.71	**0.46**	**0.88**	**0.87**	0.81	-0.59	0.05	0.80	**0.77**	**0.89**	1.00															
Ni	0.79	0.29	0.70	-0.22	0.14	0.63	0.51	0.79	0.79	0.77	-0.39	0.25	0.77	**0.68**	0.80	0.88	1.00														
Cu	0.67	0.02	**0.69**	-0.44	-0.36	0.43	0.03	**0.73**	0.71	0.71	-0.49	-0.03	0.76	**0.53**	**0.79**	0.74	0.66	1.00													
Zn	0.91	-0.02	0.80	-0.62	-0.15	0.70	0.38	**0.92**	0.93	0.87	-0.74	-0.15	0.84	**0.73**	**0.94**	0.85	0.74	0.71	1.00												
Ga	**0.96**	0.00	**0.89**	-0.59	-0.13	0.80	**0.43**	**0.99**	0.99	0.91	-0.72	-0.06	0.88	**0.76**	**0.99**	**0.89**	**0.81**	**0.76**	**0.94**	1.00											
Y	**0.90**	-0.07	**0.87**	-0.60	-0.20	0.81	**0.37**	**0.98**	0.96	0.90	-0.72	-0.06	0.81	**0.63**	**0.95**	0.86	**0.77**	**0.73**	**0.89**	**0.96**	1.00										
Nb	**0.93**	-0.05	**0.89**	-0.60	-0.20	**0.81**	**0.38**	**0.99**	0.99	0.91	-0.73	-0.09	0.85	**0.68**	**0.98**	**0.87**	**0.79**	**0.75**	**0.92**	**0.99**	**0.98**	1.00									
Ta	**0.92**	-0.03	**0.88**	-0.57	-0.17	**0.80**	**0.41**	**0.98**	**0.98**	**0.90**	-0.72	-0.08	**0.84**	**0.68**	**0.97**	**0.87**	**0.81**	0.76	**0.91**	**0.98**	**0.98**	**0.99**	1.00								
Zr	**0.92**	-0.06	**0.89**	-0.63	-0.15	0.85	0.42	**0.98**	0.96	0.89	-0.74	-0.06	0.79	**0.64**	**0.94**	0.85	0.75	0.69	**0.89**	**0.96**	**0.98**	**0.98**	0.97	1.00							
Hf	**0.90**	-0.05	**0.87**	-0.62	-0.09	**0.87**	**0.48**	**0.97**	0.,96	0.87	-0.73	-0.07	**0.74**	**0.61**	**0.92**	**0.83**	**0.74**	0.66	**0.88**	**0.94**	**0.97**	**0.97**	0.96	**0.99**	1.00						
Mo	-0.30	0.30	-0.26	**0.27**	**0.36**	-0.35	0.05	-0.34	-0.34	-0.31	0.66	0.21	-0.26	-0.01	-0.32	-0.16	-0.02	-0.17	-0.30	-0.32	-0.34	-0.35	-0.33	-0.37	-0.36	1.00					
Sn	**0.93**	-0.04	**0.87**	-0.63	-0.21	**0.72**	**0.34**	**0.96**	**0.96**	**0.88**	-0.73	-0.13	**0.88**	**0.78**	**0.98**	**0.87**	**0.76**	0.79	**0.95**	**0.97**	**0.91**	**0.95**	0.94	**0.91**	0.89	-0.31	1.00				
Tl	**0.93**	-0.04	**0.90**	-0.65	-0.14	**0.81**	0.43	**0.98**	**0.98**	**0.88**	-0.73	-0.06	**0.80**	**0.74**	**0.96**	**0.88**	**0.78**	0.75	**0.91**	**0.97**	**0.96**	**0.98**	**0.98**	**0.96**	**0.96**	-0.32	**0.95**	1.00			
Pb	0.59	-0.03	**0.43**	-0.64	-0.32	0.28	0.03	**0.53**	0.55	0.45	-0.58	-0.27	0.50	0.71	0.57	0.50	0.26	0.46	**0.61**	0.55	0.47	0.51	0.50	**0.46**	0.42	-0.18	0.66	0.57	1.00		
U	-0.33	0.47	-0.31	**0.30**	**0.44**	-0.38	0.08	-0.39	-0.40	-0.36	0.67	0.31	-0.31	0.00	-0.38	-0.13	-0.01	-0.22	-0.36	-0.38	-0.40	-0.41	-0.39	-0.42	-0.42	0.94	-0.37	-0.37	-0.22	1.00	
Th	**0.91**	-0.04	**0.88**	-0.66	-0.14	**0.85**	**0.44**	**0.98**	0.96	0.87	-0.73	-0.07	**0.76**	**0.65**	**0.93**	**0.85**	0.74	0.69	**0.89**	**0.96**	**0.98**	**0.98**	**0.97**	**0.99**	**0.99**	-0.35	**0.91**	**0.97**	0.49	-0.40	1.00
REE	0,90	-0,04	**0,87**	-0,63	-0,16	**0,85**	0,42	0,97	0,96	0,87	-0,73	-0,04	0,76	0,63	0,93	0,85	0,75	0,69	0,88	0,95	0,99	0,98	0,97	**0,99**	0,99	-0,35	0,90	0,96	0,46	-0,40	0,99	1,00

Statistical significance shown in bold was calculated combining effect size values (Pearson's r and Cohen's d) with confidence intervals (CIs). Effect size 'small' ($r = 0.1$, $d = 0.2$) 'medium' ($r = 0.3$, $d = 0.5$) and 'large' ($r = 0.5$, $d = 0.8$) (Cohen 1988)

Table 3 Factor loadings of the principal component analysis from the Zoñar Lake sedimentary record

	Comp1	Comp2	Comp1′	Comp2′
Importance of components				
SD	2.0935	1.1734	1.9858	1.3520
Proportion of variance	0.5478	0.1721	0.4929	0.2285
Cumulative proportion	0.5478	0.7200	0.4929	0.7214
Loadings				
Al	−0.369	−0.400	−0.337	−0.439
Si	−0.450		−0.469	−0.114
S	0.274	−0.489	0.232	−0.437
K	−0.441		−0.472	
Ca	−0.193	−0.508	−0.137	−0.459
Ti	−0.425	0.238	−0.444	0.215
Mn		0.443		0.464
Fe	−0.414	0.274	−0.412	0.349

Comp1 and 2: PCA analyses using dataset with 1,699 cases
Comp1′ and 2′: PCA analyses using dataset with 53 cases

presence of clay minerals, quartz, feldspar and detrital calcite.

2. *Endogenic carbonate component* identified by high Mg, TIC and TOC values and associated with dolomite, high-magnesium calcite, aragonite and Sr.
3. *Evaporite component* defined by S and gypsum.

The first three components of the PCA explain 64.61% of the total variance of the geochemical dataset: the first eigenvector accounts for 37.22%, the second for 15.78% and the third for 11.60% of the total variance. The rest of the components defined by PCA show percentages of variance <7%. Principal component 1 (PC1) is tied at the negative end by the allochthonous component and at the positive end by the evaporite and endogenic carbonate components. PC2 is controlled by S at the positive end and by TOC, TIC, Mg and Ba at the negative end. Aragonite and Sr showed positive values of PC3 (not shown), suggesting that aragonite precipitation could be explained by this third component.

Major elements

Qualitative (XRF scanner) and quantitative (AA) data of major elements are shown in Fig. 3. Graphic comparison of elemental profiles obtained by the two techniques shows a good fit, except for Al, which is not accurately measured by XRF (Rothwell and Rack 2006). The good fit supports the use of element counts (cps) obtained by XRF as a reliable measure of chemical element variations, as shown previously (Brown et al. 2007; Moreno et al. 2007). Al, Si, K, Ti

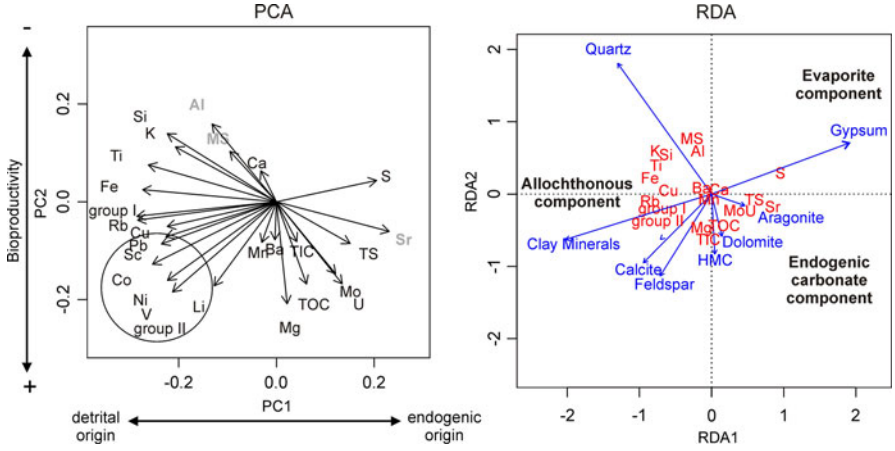

Fig. 2 Comparison of distribution of geochemical composition (TOC, TIC, TS, major, trace elements and REE) and PCA biplot and distribution of these variables constrained to mineralogical composition (calcite, quartz, clay minerals, feldspar, aragonite, dolomite, HMC and gypsum) -RDA biplot-. Dataset contains 26 variables and 53 cases for PCA and 35 variables and 53 cases for RDA. The first PCA eigenvector highlights the detrital input versus endogenic precipitation, whereas the second eigenvector has been interpreted as changes in biological productivity and sediment delivery. Aragonite, Sr, Al, MS and Quartz are shown in grey, representing positive values of the third eigenvector, which indicates saline to brackish lake environments

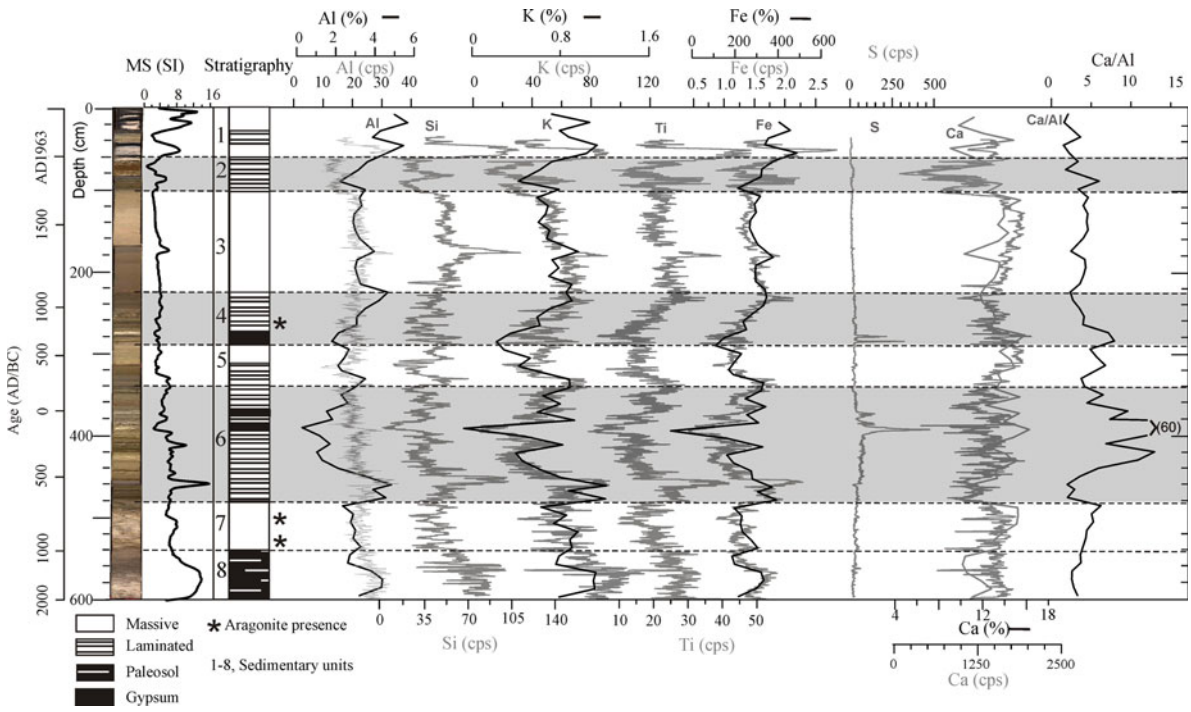

Fig. 3 Geochemical stratigraphy of Zoñar Lake core ZON04-1B. Major elements (Al, Si, K, Ti, Fe, S and Ca) measured by XRF core scanner (*grey profiles*) are expressed as counts per second (cps) and quantitative measurements by Atomic Absorption (Al, K, Fe and Ca) are expressed as percentages (*black profiles*). Ca/Al ratio is included. Age (AD/BC) was based on AMS ^{14}C and ^{137}Cs dating. *Grey bands* indicate laminated units. Sediment units 1 to 8 are defined in Martín-Puertas et al. (2008)

and Fe are associated with siliciclastic minerals of the calcite mud (allochthonous component), so this relationship is more evident in massive units than in the laminated sediments (Fig. 3), where the compositional variability occurs at millimeter scale (Table 1). Ca has a more complex pattern because it has several sources, and can be associated with minerals of different origins, such as detrital and endogenic carbonates, and gypsum. To clarify the nature of Ca in the sediments, it was normalized to Al. The Ca/Al profile shows high and constant values in massive units, following a trend similar to Al, Si, K, Fe, Ti, but shows a larger range in laminated units. Micro-XRF analyses (54-μm resolution) and microscopic description showed that the Ca peaks in unit 6 represent endogenic calcite layers (Martín-Puertas et al. 2009). Mg/Ca and Sr/Ca ratios (Fig. 4) also support carbonate precipitation in units 2, 4, 6 and 7 because lacustrine endogenic carbonates are Mg- and Sr-enriched (Dickson et al. 1990). Mn variability is low and was normalized to allochthonous elements (Mn/Fe ratio) showing maximum values in laminated sediments of unit 2, 4 and 6 (Fig. 4). The Si profile is similar to the allochthonous element profiles, indicating a predominantly detrital source. In unit 2, where Si and biogenic silica display opposite behaviors, diatoms are probably a major Si source (Fig. 3).

Trace elements

Most of the analyzed trace elements are included in groups I and II, and along with Al, Si, K, and Fe, represent the signal of the allochthonous component. However, some trace elements do not follow the allochthonous trend (Fig. 4) and are indicative of endogenic lacustrine processes. The Ba/Al profile, with maximum values in units 2, 4, 6 and 7 (Fig. 4), suggests the possible presence of authigenic Ba minerals in carbonates and sulphates of these units. Small amounts of barite and celestite, detected by SEM, corroborate this hypothesis. The Mg/Ca and Sr/Al peaks are also related to authigenic minerals: Sr to aragonite (Fig. 2) in units 7 and 4 and to calcite layers at the micro-scale in laminated sediments of

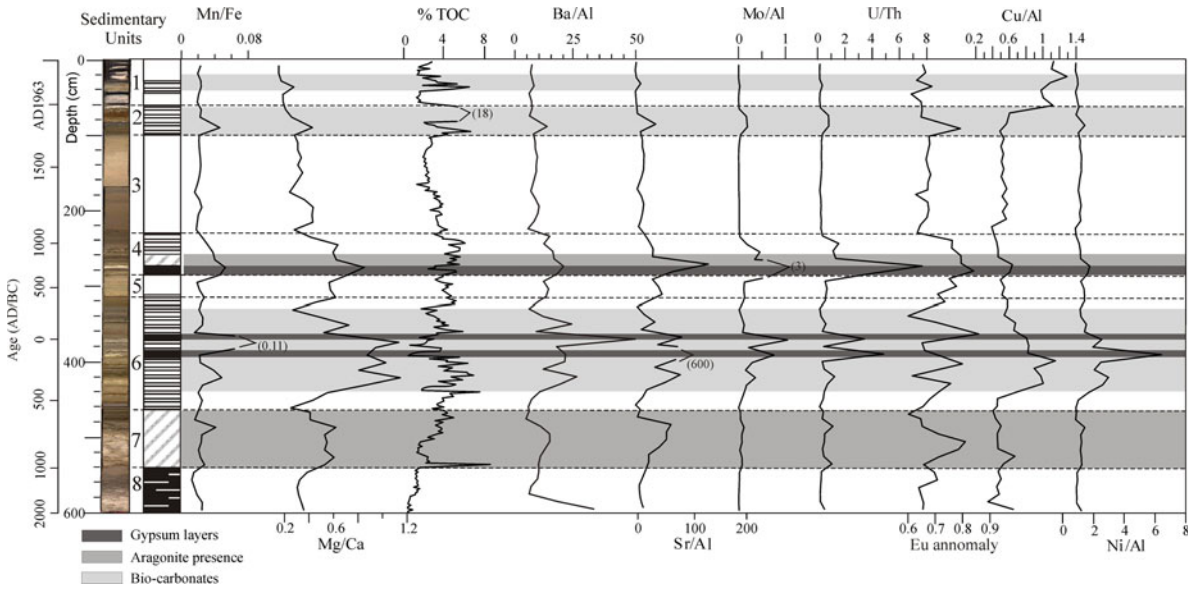

Fig. 4 Trace element ratios as indicators of lacustrine processes in Zoñar Lake. Mn/Fe, Mg/Ca and TOC: biological productivity. Ba/Al and Sr/Al: endogenic carbonate precipitation, Mo/Al, U/Th and Eu anomaly: paleo-redox proxies and Cu/Al and Ni/Al: human impact during the Iberian and Roman Epoch (450–320 cm) and the last 50 years (0–60 cm)

unit 6, and Mg to calcite (Martín-Puertas et al. 2009). The Mo/Al and U/Th ratios also show higher values in laminated units 2, 4 and 6, and likely reflect redox changes at the lake bottom, as found in other sites (Tribovillard et al. 2006 and references therein) (Fig. 4). Other metals, such as Cu, also show increases in units 1 and 6 and could be used as indicators of human influence (pollution), as pointed out previously by Valero-Garcés et al. (2006).

Rare earth elements

REEs in lacustrine sediments have shown potential as paleoenvironmental proxies because they are sensitive to pH and salinity (Sholkovitz 1992; Åström 2001), redox fluctuations (McRae et al. 1992), and changes in detrital sources (Tanaka et al. 2007). The REE characteristics of Zoñar Lake sediments, as indicated by the chondrite-normalized patterns, display no significant differences along the core. These patterns (Fig. 5) exhibit LREE enrichment and a negative Eu anomaly typical of the average composition of upper continental crust. The highest REE contents are in clay-rich unit 1, and the relatively lower REE contents of the rest of the sequence can be explained by the diluting effect of carbonates and sulphates. Lower REE abundance than North

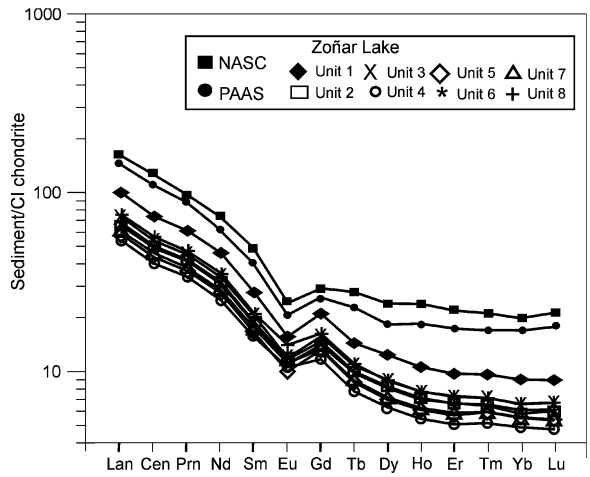

Fig. 5 REE chondrite-normalized patterns of Zoñar Lake sediments compared with standard REE pattern of North American and Australian shale. REE patterns of Zoñar sediments exhibit a typical variation, but show a weak depletion of HREE compared to NASC and PAAS. Sedimentary units 1 to 8 are defined in Martín-Puertas et al. (2008)

American shale composite (NASC) and Post-Archean Australian average shale (PAAS) (Fig. 5) also reflects the carbonate nature of the Zoñar Lake sediments.

The statistical significance of the relationship between Al-REE and K-REE (Table 2) suggests that siliciclastic minerals are the major REE hosts,

probably clay minerals and also minor phases such as zircon (REE-Zr). The uniform REE patterns and similar (La/Yb) fractionation values, with an average value of 11.26 along the core, reflect a similar lithological source area and no changes in either the detrital component or the weathering processes and intensity along the sequence (McLennan 1989). A clear, but almost uniform depletion in HREE can be observed when compared with the PASC or NASC. This weak fractionation may be interpreted as inherited from the source area and probably related to the carbonate nature of the sediments. Figure 4 shows the Eu/Eu* profile, in which several units have values >0.65 (average value for upper continental crust, UCC). In the absence of changes in source materials and weathering of bedrock, the observed values likely indicate diagenetic processes that can change the Eu oxidation state according to fluctuating redox conditions (McRae et al. 1992).

Discussion

Watershed processes and paleoenvironmental significance

The first eigenvector of the PCA highlights the differences between the terrigenous component and the authigenic (evaporite and endogenic carbonate) sediment components and can thus be interpreted as indicative of changes in sediment supply, lake level and salinity (Fig. 2). Concentrations of Sr, gypsum and aragonite are indicative of greater ion concentrations in the water during low lake levels. Higher lake levels are characterized by sediments with greater amounts of clay minerals and quartz.

At a basin scale, there are two main watershed processes affecting Zoñar Lake: (1) soil development during periods of sub-aerial exposure, and (2) detrital input to the lake, delivered via runoff from small creeks. The unique geochemical composition of unit 8 confirms that lake sediments were affected by soil-forming processes during a sub-aerial exposure period prior to 950 BC (Martín-Puertas et al. 2008). From top to bottom, three intervals can be identified that correspond to soil horizons (FAO 1998) (Fig. 6a): (1) a top layer with high TOC content (horizon Ah); (2) an intermediate layer with very high Si and quartz content, caused by eluviation processes (horizon E); and (3) a basal layer characterized by Si decrease, but high clay accumulation, indicative of illuvial processes (horizon Bt) (Maher 1998).

The two types of detrital facies, identified by sediment properties (Fig. 6b), have different geochemical signatures. The first type is composed of massive, thick layers in units 5, 3 and 1 that are characterized by moderate values of the allochthonous component and high Ca (Fig. 6b). Pollen data from Martín-Puertas et al. (2008) showed a decrease in the Mediterranean forest and an increase in *Olea* during deposition of massive sediments of unit 5, and at the base of both units 3 and 1. Therefore units 5, 3 and 1 may represent an increase in the clastic delivery to the lake during three periods of more intense farming, the Muslim Epoch (AD 600–1100), the Middle Ages after the Christian conquest of the Guadalquivir Valley (after AD 1200), and the second half of the 20th century, after agricultural mechanization.

The second type is represented by thin layers of coarser sediments, with high quartz and clay mineral content, high magnetic susceptibility values, and fining-upward textures. These features suggest deposition during short time intervals, associated with flood events in the basin, as has been shown in other lakes (Noren et al. 2002; Moreno et al. 2008). The geochemical signature is characterized by sharp peaks in allochthonous components. Based on the age-depth model for Zoñar Lake (Martín-Puertas et al. 2008), short periods of increased sediment delivery to the lake occurred at 650 BC, 300 BC, AD 300–370, AD 1350, and two episodes during the last century (1950–1970 and after 1980). The two intervals with the highest magnetic susceptibility and allochthonous component values, at 650 BC and AD 1350, coincide with global Rapid Climate Change periods defined by Mayewski et al. (2004) as shifts to humid conditions. They also correspond to two unique "lake transgression" periods in the Zoñar Basin, with flooding of the whole basin at 650 BC, and re-flooding of the shallower NW sub-basin at AD 1350 (Martín-Puertas et al. 2008).

Endogenic lacustrine processes

Sediment facies and mineralogical analyses show that sulfates (gypsum, barite and celestite), sulfides (pyrite

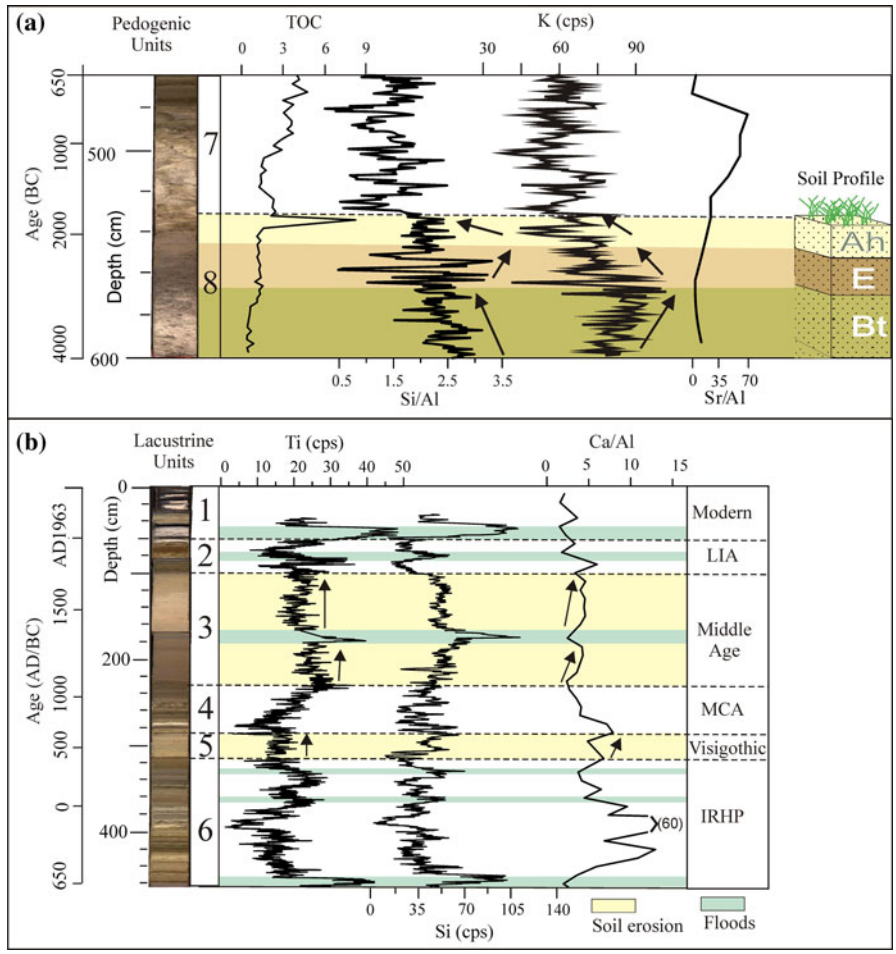

Fig. 6 Geochemical signature of the main watershed processes in Zoñar Lake. **a** soil development in unit 8 and Sr increase as an indicator of aragonite precipitation during ephemeral lake conditions. **b** periods of increased littoral erosion with allochthonous component (indicated by Ti) enriched in Ca, and periods of flooding characterized by allochthonous component with high Si content

traces) and carbonates (aragonite, calcite and high-Mg calcite) are the only endogenic minerals precipitating in the lake and/or in the sediment column. The second eigenvector can be interpreted as indicative of the intensity of the biological processes in the lake. Negative values correlate with high productivity (high TOC) and with the endogenic carbonate component, and positive values with low organic productivity and predominance of the evaporite component (gypsum). Higher productivity and preservation of organic matter occurred during deposition of laminated facies, generally during higher lake levels. On the other hand, this eigenvector is related to fine terrigenous input (clays) at the negative end, and coarser siliciclastic deposition at the positive end, indicating their different hydrodynamic behaviors. A similar situation has been pointed out in other hypersaline Spanish (Gallocanta, Rodò et al. 2002) and Central Asian (Caspian Sea—KaraBogaz Gol, Giralt et al. 2003) lacustrine ecosystems.

Some geochemical indicators allow a better characterization of these processes. The high Sr/Al peaks in unit 6 coincide with evaporite (gypsum) formation during high salinity stages when carbonates do not precipitate (Fig. 4). The absence of carbonates in these layers suggests that Sr precipitates as sulfate (celestite), coetaneous with gypsum. Although low presence (<5% wt) or low crystallinity of these minerals does not allow detection of Sr or Ba sulfates by XRD analysis, scanning electron microscopy revealed the presence of micron-size celestine and barite crystals in these layers. Sr is preferentially taken up by aragonite and Mg is incorporated by calcite, HMC and dolomite (Cohen 2003), and it is clearly associated with aragonite-rich intervals (Fig. 4). Ba enrichment (Ba/Al) in unit 7, together with Sr/Al peaks in aragonite

phases (Fig. 4), indicates Ba precipitation associated with carbonates and sulfates, likely as Ba^{2+} substituting for Ca^{2+} in the aragonite structure (Dickson 1990), and as barite that precipitated in smaller amounts, as it also occurs at unit 6 and 4.

In many lakes, calcite precipitation is induced by photosynthetic activity, resulting in a pH rise. However, a unique geochemical indicator for productivity is elusive. Biogenic silica is commonly used as a paleoproductivity proxy (Cohen 2003; Bertrand et al. 2008) if it can be assumed that its accumulation is proportional to diatom productivity and is a reflection of total primary productivity in the lake (Cohen 2003). Under high pH conditions, however, dissolution of diatom frustules occurs and the presence of reworked marine diatoms in the Zoñar Lake sediments precludes the use of biogenic silica as a lacustrine productivity indicator. Organic carbon content can also be used as a paleoproductivity indicator (Meyers 1997), although there is evidence of oxidation processes, for instance in unit 3, which favor the degradation of organic matter (Demaison and Moore 1988). In Zoñar Lake, Mn/Fe and Mg/Ca ratios can be considered reliable paleoproductivity indicators. Higher Mn/Fe occurs in sediments of higher organic matter content, and Mg/Ca reflects more biologically-induced carbonate precipitation.

The three eigenvectors of the PCA could be interpreted as a sequence of increasing lake level that follows a complex sedimentological pattern: (1) the most saline lake conditions, with gypsum formation, are represented by samples at the negative end of eigenvector 1 and the positive end of eigenvector 2; (2) the first stages of lake level increase, favoring the formation of aragonite (high salinity conditions due to the dissolution of the salt pan), are marked by samples at the positive end of eigenvector 3; (3) the transition to fresher conditions, with increased allochthonous input, are represented by samples located at the positive end of eigenvector 1, and (4) the highest lake level and freshest conditions, coinciding with the highest biological productivity (high total organic carbon and biogenic silica content), as in unit 6, are marked by samples at the negative end of eigenvector 2. Examples of lake-level increase sequences occur in unit 4 and at the transition from unit 7 to 6. Sequences of lake level decline are less clear, but occur during the gypsum interval in unit 6 and at the transition from unit 5 to 4.

Paleo-redox conditions

A wide variety of trace metals have been used as proxies for paleo-redox conditions in marine and continental environments: Mn, U, V, Mo, Ni, Cr, Ni, Co (Solhenius et al. 2001; Calvert and Pedersen 1993; Martínez-Ruiz et al. 2000; Gallego-Torres et al. 2007). U and Mo are conservative in oxic environments, but are enriched in anoxic sediments (Morford and Emerson 1999; Chaillou et al. 2002; Sundby et al. 2004; Elbaz-Poulichet et al. 2005). To choose the most suitable paleo-redox proxies in Zoñar Lake, a correlation with Al was used to eliminate those elements controlled by detrital influx, and to identify elements related exclusively to redox conditions at the lake bottom (Tribovillard et al. 2006). The Mo and U content and the Eu/Eu* anomaly do not show any correlation with detrital input and likely reflect changes in redox conditions (Fig. 4).

While Mo/Al, U/Th, Mn/Fe ratios display very similar profiles, Eu/Eu* is out of phase with these indicators in unit 4 and at the base of unit 2. Eu/Eu* positive anomalies are well correlated with the Ba/Al increase. On the other hand, the Eu anomaly varies along the core (Fig. 4) and higher Eu anomaly values at the base of the sequence could be related to clay-enrichment processes in the soil profile in a highly reducing environment. The rest of the values above the PAAS-NASC Eu anomaly value, occur in laminated intervals with gypsum or carbonate precipitation, i.e. units 6, 4 and 2. Among the REE, only Ce and Eu change their oxidation state according to redox conditions, which can cause a unique and anomalous behavior compared with other REEs. The close relation between the Eu anomaly and the laminated intervals suggests a strong lacustrine environmental control of the redox state of Eu. Among the different processes that can fractionate REE, low oxidation potential, especially in organic-rich sediments, is the most significant, leading to increased REE solubility, enrichment of pore waters in Eu^{2+}, and positive Eu anomalies in the sediments (Lev and Filer 2004; Abanda and Hannigan 2006). At some sediment depths, lower values of organic matter coincide with a positive Eu anomaly (e.g. unit 2, and the gypsum-rich interval in unit 6) (Fig. 4). These intervals could indicate short-lived periods of aerobic respiration and oxygen consumption. The association

of these levels with detrital input suggests inflow of oxygenated waters into the lake or minor lake level fluctuations that caused oxygenation events within a predominantly anoxic period.

Down-core proxy paleo-redox profiles show an alternation between oxic and anoxic environments at the bottom of the lake. Oxic conditions in the sediment prevailed during: (1) the period of sub-aerial exposure in units 8 and the lower half of unit 7, and (2) during deposition of massive sediments in units 1, 3 and 5, during generally lower lake level and well-mixed conditions. Anoxic conditions occurred during the periods of high organic productivity (high Mg/Ca and Fe/Mn), and high preservation potential for lamination (units 6, 4, 2 and 1), similar to those described by Tribovillard et al. (2006), but also during hypersaline conditions, indicated by gypsum presence. Anoxic lake bottom conditions during gypsum precipitation, as occur in units 4 and 6, are common in shallow and deep hypersaline lakes (Last and Vance 2002) where gypsum layers may play a boundary role for oxygen diffusion through the sediment–water interface, increasing anoxia in underlying sediments.

Lacustrine geochemical signatures during the Late Holocene

High-resolution geochemical analyses of the Zoñar Lake sediment sequence enhance the previous paleohydrological and paleoenvironmental reconstructions based on sedimentological, mineralogical and biological proxies (Valero-Garcés et al. 2006; Martín-Puertas et al. 2008, 2009).

One of the most conspicuous features of the Zoñar Lake multi-proxy reconstruction (Martín-Puertas et al. 2008) is the succession of wet and dry conditions at a centennial-scale, generally synchronous with rapid climate changes that occurred in Europe and the Mediterranean during the late Holocene (Mayewski et al. 2004). In Zoñar Lake, arid phases are identified prior to 950 BC, during the 150 BC–AD 150 Roman Epoch, and during AD 800–1300 (MCA). More humid conditions occurred during the Iberian and Roman period (IRHP, 550 BC–AD 300), during the Christian conquest of the Guadalquivir Valley around AD 1300, and during several intervals in the Little Ice Age (AD 1400–1850, Valero-Garcés et al. 2006; Martín-Puertas et al. 2008).

The geochemical signatures of more humid periods are exemplified by the IRHP (Fig. 7a). Higher lake levels are conducive to seasonally and/or permanently stratified waters with bottom anoxia, indicated by U/Th, Mo/Al ratios and the Eu anomaly, and higher biological productivity, as indicated by higher Mg/Ca and Mn/Fe ratios (Fig. 7a2). Heavy metal increases (Ni/Al, Fig. 4) are interpreted as early human influences (e.g. metallurgy and smelting) in the area. This period, however, is unique in the history of the lake, since other relatively humid periods, such as the onset of the Little Ice Age (LIA) around AD 1400, the re-flooding of the NW sub-basin around AD 1600, and some times during the period AD 1800–1900 (Valero-Garcés et al. 2006; Martín-Puertas et al. 2008, 2009), do not show similar sedimentological, mineralogical and geochemical features.

On the other hand, geochemical indicators S and Sr/Al identify clearly the salinity increases during the aridity crisis of the third millennium BP (drying of the lake and soil development) (Fig. 6a), the 300-year deposition of gypsum from 150 BC to AD 150 (Imperial Roman Epoch) (Fig. 7a3), the Medieval Climate Anomaly (Fig. 7b), and the late 19th century (Fig. 4).

The end of the humid IRHP (AD 350) is characterized by geochemical indicators of lower productivity (decreases in Mg/Ca and Mn/Fe ratios), and increases in clastic input to the lake (Fig. 6b). This increase in sediment delivery to the lake during the Decline of the Roman Empire is unlikely to have resulted from increased farming or land use change. This change more likely reflects a trend toward more arid conditions that led to lower lake levels and increasing littoral erosion and sediment delivery to the lake. The aridification trend continues in unit 4 (AD 600–1200) during the MCA, (AD 800–1300, Jones et al. 2001), when salinity increased (increasing Sr/Al ratios) (Fig. 7a, b), with frequent periods of anoxic bottom sediment (higher Mo/Al, U/Th and Eu anomaly) (Fig. 4). Preservation of laminae and higher organic productivity at the end of this period of high ion concentrations in waters could have been a direct response to lower sediment delivery to the lake (lower turbidity), similar to what occurred during

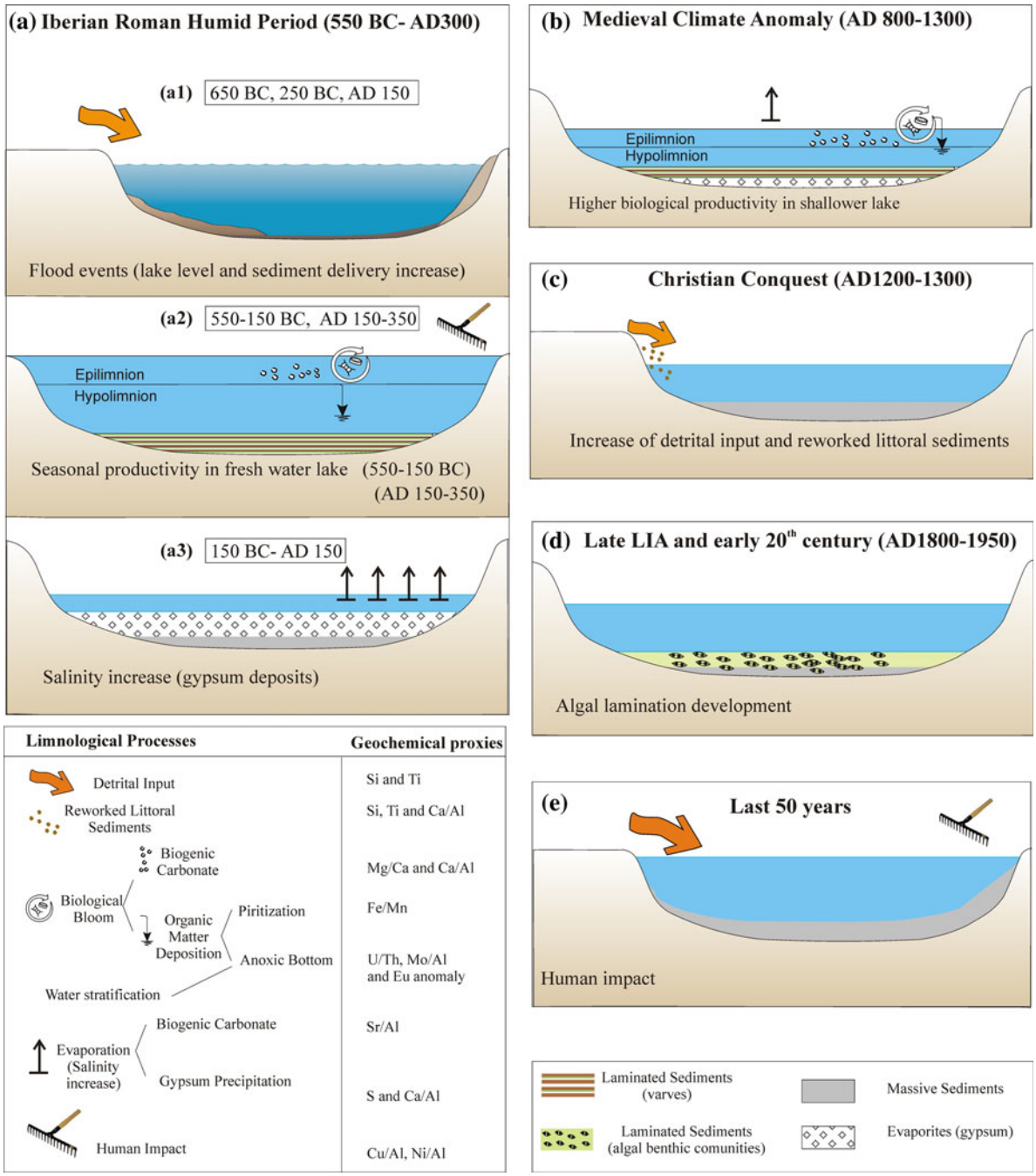

Fig. 7 Geochemical proxies (elements and ratios) in Zoñar Lake core sediments during the climatic and cultural periods of the Late Holocene. Watershed erosion shown as Si–Ti increases can be a consequence of: precipitation increase as during the IRHP (**a1**); increased erodibility during periods of reduced vegetation cover (**c**); and soil erosion caused by human impact (**d**). Endogenic processes include: (1) biological activity enhanced during higher lake level and thermal stratification with varve preservation (**a2**) or better development of benthic communities during lower lake levels (**d**); (2) anoxia in the sediments as consequence of permanent water stratification conditions or organic matter degradation after a '*bloom*' (**a3**, **b**, **d**), and (3) gypsum and chemical carbonate precipitation as a result of negative water balance and chemical concentration (**a3**, **b**)

deposition of laminated facies around AD 800 (Fig. 7b).

The geochemical signatures of the LIA (Fig. 7d) (AD 1300–1900, Jones et al. 2001) in the Zoñar sequence are complex because of the occurrence of several arid and humid phases and intense human impact in the watershed since Medieval times. Geochemical signatures of lake level rise identified by sedimentological and biological proxies at the onset of the LIA and around AD 1600 (Martín-Puertas et al. 2008) are unclear, and do not show similarities with the earlier, high lake level period of the IRHP. Much higher sediment delivery than during Iberian-Roman times could have had a negative impact on the biological development of algal blooms, restricting development of laminated facies. Only when sediment delivery sharply decreased (AD 1800–1950) (unit 2), did biological activity in Zoñar Lake reach values similar or even higher than those during the IRHP, with the highest values of total organic carbon, Mg/Ca and Mn/Fe (Figs. 4; 7d). Redox indicators during the past two centuries show an alternation of oxic and anoxic conditions that correlate with massive and laminated facies, respectively (Fig. 7d). Biological indicators point to relatively shallower conditions. Diatom assemblages during laminated unit 2 (Valero-Garcés et al. 2006) are dominated by benthic species, and the presence of algal mats is indicative of oxic bottom conditions with enough light for photosynthesis (Fig. 7d). Anthropogenic forcing (i.e. less sediment delivery, increased human use of the water) seems to have played a role in the development of laminated facies during this phase.

Since the mid 1950s, another phase of increased detrital input occurred (Fig. 7e). During this period, lake sediments became enriched in metals (Cu) (Fig. 4), reflecting the increased use of fertilizers in the watershed. The deposition of faintly laminated, organic-rich facies during AD 1970–1980 is synchronous with: (1) reduced annual precipitation and warmer summer temperatures, (2) greater consumptive use of the Zoñar springs until 1980, and (3) a decrease in farming in some areas of Andalusia, though still undocumented in the Zoñar watershed. The synergistic effects of these processes seem to have led to lower water levels in Zoñar Lake and better conditions for deposition of algal-rich, laminated facies.

Geochemical signatures in the sediments of Zoñar Lake reflect paleolimnological variability and a response to the interplay between climate and anthropogenic changes during the last few millennia. For example, during the IRHP, high lake level (humid conditions) prevailed, and sediment delivery to the lake was relatively low (Fig. 7a). The most intense farming during the Roman Empire Epoch (150 BC–150 AD) coincided with a relatively dry phase at a regional scale. The second most intense agricultural phase started with the Christian conquest of the Guadalquivir River Valley (AD 1200–1300) and it was synchronous with the end of the MCA. Since AD 1950, mechanization of farming activities and increased use of fertilizers (Cu/Al) mark the largest increase in soil erosion and sediment delivery to the lake (Fig. 7e).

Societal crises and associated land use changes (farming and shepherding) had strong impacts on lacustrine processes. For example, crises at the end of the Visigoth period (7th century AD) and during the 19th century contributed to reduced sediment delivery to the lake, lowered water turbidity, and increased biological productivity.

Conclusions

High-resolution geochemical data from the Zoñar Lake sediment sequence enhance previously inferred hydrological reconstructions and provide a detailed history of the sediment regime, past redox conditions, and chemical evolution of the lake. Detrital inputs represent flooding episodes and are expressed by Si-, Al-, K-, Ti- and Fe-enriched sediments, while Ca-rich allochthonous sediments are indicative of reworked sediments during drier periods or lake level fluctuations. The Sr/Al profile shows ion-rich waters and chemical mineral precipitation, e.g. aragonite and gypsum, during saline and brackish lake stages. Greater productivity is marked by higher organic carbon content and higher carbonate precipitation (Mg/Ca). Endogenic calcite precipitation (chemically or biologically induced) is also indicated by higher Ca/Al, Sr/Al and Ba/Al ratios. Heavy metal enrichment in the sediments (Cu and Ni) suggests intensification of human activities during the Iberian Roman Period and the use of fertilizers during the last 50 years. Mo/Al and U/Th ratios and Eu anomalies

mark shifts in the state of lake bottom oxygenation. Thus, the geochemical composition of lake sediments provides detailed information about lacustrine and watershed processes, and reflects natural (i.e. climatic) and human influences over the last 4,000 years.

Acknowledgments Financial support for this study was provided by the Spanish Ministry of Science and Education (Projects GRACCIE CSD2007-00067, IBERLIMNO CGL2004-20236-E, CALIBRE CGL2006-13327-C04/CLI, Ministerio MARM 200800050084447 and CGL-2006-2956-BOS), an Andalusian Government Predoctoral Fellowship, and the Andalusian Government (PAI groups RNM-328 and RNM-179). We thank the LRC (University of Minnesota, USA), particularly Doug Schnurrenberger, Mark Shapley and Anders Noren, for making possible the 2004 expedition. Karin Koinig, Achim Brauer and Bernd Zolitschka provided constructive criticisms and suggestions. We also thank Mark Brenner for language editing. A. Moreno acknowledges funding from the European Commission's Sixth Framework Program (Marie Curie Outgoing International Fellowships, proposal 021673-IBERABRUPT). F. Jiménez-Espejo acknowledges the Japan Society for the Promotion of Science (JSPS).

References

Abanda PA, Hannigan RE (2006) Effect of diagenesis on trace element partitioning in shales. J Geochem Explor 91:41–55

Armstrong JS (2007) Significance tests harm progress in forecasting. Int J Forecasting 23:321–327

Åström M (2001) Abundance and fractionation patterns of rare earth elements in streams affected by acid sulphate soils. Chem Geol 175:249–258

Battarbee RW (2000) Paleolimnological approaches to climate change, with special regard to the biological record. Quat Sci Rev 19:107–124

Bea F (1996) Residence of REE, Y, Th and U in granites and crustal protoliths: implications for the chemistry of crustal melts. J Petrol 37:521–532

Bertrand S, Charlet F, Charlier B, Renson V, Fage N (2008) Climate variability of southern Chile since the Last Glacial maximun: a continous sedimentological record from Lago Puyehue (40°S). J Paleolimnol 39:179–195

Borrego C, Tchepel O, Costa AM, Martíns H, Ferreira J, Miranda AI (2006) Traffic-related particulate air pollution exposure in urban areas. Atmos Environ 40:7205–7214

Boyle J (2000) Rapid elemental analysis of sediment samples by isotope source XRF. J Paleolimnol 23:213–221

Boynton WV (1983) Cosmochemistry of the REE: meteorite studies. In: Henderson P (ed) Rare earth element geochemistry. Elsevier, Amsterdam, pp 63–114

Brown ET, Johnson TC, Scholz A, Cohen AS, King JW (2007) Abrupt change in tropical African climate linked to the bipolar seesaw over the past 55,000 years. Geophy Res Lett 34. doi:10.1029/2007GL031240

Calvert SE, Pedersen TF (1992) Organic carbon accumulation and preservation in marine sediments: how important is anoxia? In: Whelan JK, Farrington JW (eds) Productivity, accumulation and preservation of organic matter in recent and ancient sediments. Columbia University Press, New York, pp 231–263

Calvert SE, Pedersen TF (1993) Geochemistry of recent oxic and anoxic marine sediments: implications for the geological record. Mar Geol 113:67–88

Chaillou G, Anschutz P, Lavaux G, Schäfer J, Blanc G (2002) The distribution of Mo, U, and Cd in relation to major redox species in muddy sediments of the Bay of Biscay. Mar Chem 80:41–59

Cheburkin AK, Shotyk W (1996) Double-plate sample carrier for a simple total reflection X-ray fluorescence analyser. X-Ray Spectrom 25:175–178

Cohen J (1988) Statistical power analysis of the behavioral sciences. Lawrence Erlburn Associates, Hillsdale

Cohen AS (2003) Paleolimnology. The history and evolution of lake systems. Oxford University Press, New York

Demaison GJ, Moore GT (1988) Anoxic environments and oil source bed genesis. Org Geochem 2:9–31

Dickson T (1990) Carbonate mineralogy and chemistry. In: Tucker ME, Wright VP (eds) Carbonate sedimentology. Blackwell Science, Oxford, 482 pp

Dickson JAD, Smalley PC, Raheim A, Stijifhoorn DE (1990) Intracrystalline carbon and oxygen isotope variations in calcite revealed by laser microsampling. Geology 18: 809–811

Elbaz-Poulichet F, Seidel JL, Jézéquel D, Metzger E, Prévot F, Simonucci C, Sarazin G, Viollier E, Etcheber H, Jouanneau JM, Weber O, Radakovitch O (2005) Sedimentary record of redox-sensitive elements (U, Mn, Mo) in a transitory anoxic basin (the Thau lagoon France). Mar Chem 95:271–281

Enadimsa (1989) Estudio hidrogeológico de la Laguna de Zoñar. Junta de Andalucía, Sevilla

Eusterhues K, Heinrichs H, Schneider J (2005) Geochemical response on redox fluctuations in Holocene lake sediments, Lake Steisslingen, Southern Germany. Chem Geol 222:1–22

Evensen NM, Hamilton PJ, O'Nions RK (1978) Rare-earth abundances in chondritic meteorites. Geochim Cosmochim Acta 42:1199–1212

FAO (1998) World reference base for soil resources. Rap Publication, Rome

Gallego-Torres D, Martínez-Ruiz F, Paytan A, Ortega M (2007) Pliocene-Holocene evolution of depositional conditions in the eastern Mediterranean: role of anoxia vs. productivity at time of sapropel deposition. Palaeogeogr Palaeoclimatol Palaeoecol 246:424–439

Giralt S, Juliá R, Leroy S, Gasse F (2003) Cyclic water level oscillation of the KaraBogazGol Caspian sea system. Earth Planet Sc Lett 212:225–239

Giralt S, Moreno A, Bao R, Sáez A, Prego R, Valero-Garcés BL, Pueyo JJ, González-Sampériz P, Taberner C (2008) A statistical approach to disentagle environmental forcing in a lacustrine record: the Lago Chungará case (Chilean Altiplano). J Paleolimnol 40:195–215

Goodwin LD, Leech NL (2006) Understanding correlation: factors that affect the size of r. J Experimen Education 74:251–266

IGME (1988) Mapa Geológico de España, 1:50000, (serie MAGNA). Hoja 988. Puente Genil. Servicio de Publicaciones del Ministerio de Industria y energía, Madrid

Jones PD, Osborn TJ, Briffa KR (2001) The evolution of climate over the last millennium. Science 292:662–667

Koinig KA, Shotyk W, Lotter AF, Ohlendorf C, Strum M (2003) 9000 years of geochemical evolution of lithogenic major and trace elements in the sediment of an alpine lake-the role of climate, vegetation, and land-use history. J Paleolimnol 30:307–320

Kristen I, Fuhrmann A, Thorpe J, Röhl U, Wilkes H, Oberhänsli H (2007) Hydrological changes in southern Africa over the last 200 kyr as recorded in lake sediments from the Tswaing impact crater. S Afr J Geol 110:311–326 (Special Issue)

Kylander ME, Muller M, Wüst RAJ, Gallagher K, Garcia-Sanchez R, Coles BJ, Weiss DJ (2007) Rare earth element and Pb isotope variations in a 52 kyr peat core from Lynch's Crater (NE Queensland, Australia): proxy development and application to paleoclimate in the Southern Hemisphere. Geochim Cosmochim Acta 71: 942–960

Last WM, Vance RE (2002) The Holocene history of Oro Lake, one of the western Canada's longest continuous lacustrine records. Sediment Geol 148:161–184

Lev SM, Filer JK (2004) Assessing the impact of black shale processes on REE and the U–Pb isotope system in the southern Appalachian Basin. Chem Geol 206:393–406

López-Martínez C, Grimalt JO, Hoogakker B, Grützner J, Vautravers MJ, McCave IN (2006) Abrupt wind regime changes in the North Atlantic Ocean during the past 30000–60000 years. Paleoceanography 21:PA4215. doi: 10.1029/2006PA001275

Maher BA (1998) Magnetic properties of modern soils and quaternary loessic pleosols: paleoclimatic implications. Palaeogeogr Palaeoclimatol Palaeoecol 137:25–54

Marmolejo-Rodríguez AJ, Prego R, Meyer-Willerer A, Shumilin E, Cobelo-García A (2007) Total and labile metals in surface sediments of the tropical river-estuary system of Marabasco (Pacific coast of Mexico): influence of an iron mine. Mar Pollut Bull 55:459–468

Martínez-Ruiz F, Kastner M, Paytan A, Ortega-Huertas M, Bernasconi SM (2000) Geochemical evidence for enhanced productivity during S1 sapropel deposition in the eastern Mediterranean. Paleoceanography 15:200–209

Martín-Puertas C, Valero-Garcés BL, Mata MP, González-Sampériz P, Bao R, Moreno A, Stefanova V (2008) Arid and humid phases in the southern Spain during the last 4000 years: the Zoñar Lake Record, Córdoba. Holocene 18:907–921

Martín-Puertas C, Valero-Garcés BL, Brauer A, Mata MP, Delgado-Huertas A, Dulsky P (2009) Timing, structure of the post-bronze Iberian-Roman Humid period (2.6–1.6 cal yr. BP) based on the Zoñar Lake varve record (Andalucía, southern Spain) (2009). Quat Res 71:108–120

Mayewski PA, Rohling EE, Stager JC, Karlen W, Maasch KA, Meeker LD, Meyerson EA, Gasse F, van Kreveld S, Holmgren K, Lee-Thorp J, Rosqvist G, Rack F, Staubwasser M, Schneider RR, Steig EJ (2004) Holocene climate variability. Quat Res 62:243–255

Mayr C, Fey M, Haberzettl T, Janssen S, Lücke A, Maidana NI, Ohlendorf C, Schäbitz F, Schleser GH, Struck U, Wille M, Zolitschka B (2005) Palaeoenvironmental changes in southern Patagonia during the last millennium recorded in lake sediments from Laguna Azul (Argentina). Palaeogeogr Palaeoclimatol Palaeoecol 228: 203–227

McLennan SM (1989) Rare earth elements in sedimentary rocks: influence of provenance and sedimentary processes. Rev Miner 21:170–199

McRae ND, Nesbitt HW, Kronberg BI (1992) Development of a positive Eu anomaly during diagenesis. Earth Planet Sci Lett 119:585–591

Meyers PA (1997) Organic geochemical proxies of paleoceanographic, paleolimnologic and paleoclimatic processes. Org Geochem 27:213–250

Moreno A, Giralt S, Valero-Garcés BL, Sáez A, Bao R, Prego R, Pueyo JJ, Taberner C (2007) A 14 kyr record of the tropical Andes: the Lago Chungará sequence (18°S northern Chilean Altiplano). Quat Int 161:4–21

Moreno A, Valero-Garcés BL, González-Sampériz P, Rico M (2008) Flood response to rainfall variability during the last 2000 years inferred from the Taravilla lake record (Central Iberian Range, Spain). J Paleolimnol 40:943–961

Morford JE, Emerson S (1999) The geochemistry of redox sensitive trace metals in sediments. Geochim Cosmochim Acta 63:1735–1750

Nakagawa S, Cuthill IC (2007) Effect size, confidence interval and statistical significance: a practical guide for biologists. Biol Rev 82:591–605

Noren AJ, Bierman PR, Steig EJ, Lini A, Southon J (2002) Millennial-scale storminess variability in the northeast United States during the Holocene epoch. Nature 419:821–824

Nriagu JO (1996) A history of global metal pollution. Science 272:223–224

Piper DZ, Perkins RB (2004) A modern vs Permian black shale—the hydrography, primary productivity, and water-column chemistry of deposition. Chem Geol 206:177–197

R Development Core Team (2006) R: a language and environment for statistical computing, R Foundation for Statistical Computing, Vienna

Renberg I (1986) Concentration and annual accumulation values of heavy metals in lake sediments: their significance in studies of the history of heavy metal pollution. Hydrobiologia 143:379–385

Rodò X, Giralt S, Burjachs F, Comín FA, Tenorio RG, Juliá R (2002) High-resolution saline lake sediments as enhanced tools for relating proxy paleolake records to recent climatic data series. Sediment Geol 148:203–220

Röhl U, Brinkhuis H, Fuller M (2004) On the search for the Paleocene/Eocene boundary in the southern Ocean: exploring ODP Leg 189 Holes 1171D and 1172D. In: Exon NF, Malone M, Kennett JP (eds) The Cenozoic southern ocean and climate change between Australia and Antarctica. American Geophysical Union, Geophysical Monograph Series, 181, pp 113–126

Rosenthal R, Rubin DB (1986) Meta-analytic procedures for combining studies with multiple effect sizes. Psychological Bull 99:400–406

Rothwell RG, Rack F (2006) New techniques in sediment core analysis: an introduction. In: Rothwell RG (ed) New techniques in sediment core analysis. The Geological Society of London, London, pp 1–29

Ruiz-Fernández AC, Páez-Osuna F, Urrutia-Fucugauchi J, Preda M (2007) ^{210}Pb geochronology of sediment accumulation rates in Mexico City metropolitan zone as recorded at Espejo de los Lirios lake sediments. Catena 61:31–48

Sánchez M, Fernández-Delgado C, Sánchez-Polaina FJ (1992) Nuevos datos acerca de la morfometría y batimetría de la laguna de Zoñar (Aguilar de la Frontera, Córdoba). Oxyura 6:73–77

Schettler G, Romer RL (2006) Atmospheric Pb-pollution by pre-medieval metallurgy detected in the sediments of the brackish karst lake An Loch Mór, western Ireland. App Geochem 21:58–82

Selig U, Leipe T, Dörfler W (2007) Paleolimnological record of nutrient and metal profile in prehistoric, historic and modern sediments of three lakes in north-eastern Germany. Water Air Soil Poll 184:183–194

Sholkovitz ER (1992) Chemical evolution of rare earth elements: fractionation between colloidal and solution phases of filtered river water. Earth Planet Sci Lett 114:77–84

Sholkovitz E, Szymczak R (2000) The estuarine chemistry of rare earth elements: comparison of the Amazon, Fly, Sepik and the Gulf of Papua systems. Earth Planet Sci Lett 179:299–309

Solhenius G, Emeis KC, Andrén E, Andrén T, Kohly A (2001) Development of anoxia during the Holocene fresh-brackish water transition in the Baltic Sea. Mar Geol 177:221–242

Sundby B, Martínez P, Gobeil C (2004) Comparative geochemistry of cadmium, rhenium, uranium, and molybdenum in continental margin sediments. Geochim Cosmochim Acta 68:2485–2493

Tanaka K, Akagawa F, Yamamote K, Tani Y, Kawabe I, Kawai T (2007) Rare earth elements geochemistry of Lake Baikal sediment: its implication for geochemical response to climate change during the Last Glacial/Interglacial transition. Quat Sci Rev 26:1362–1368

Tribovillard N, Algeo TJ, Lyons T, Riboulleau A (2006) Trace metals as paleoredox and paleoproductivity proxies: an update. Chem Geol 232:12–32

Valero-Garcés BL, González-Sampériz P, Navas A, Machín J, Mata P, Delgado-Huertas A, Bao R, Moreno A, Carrión JS, Schwalb A, González-Barrios A (2006) Human impact since medieval times and recent ecological restoration in a Mediterranean lake: the Laguna Zoñar, southern Spain. J Paleolimnol 35:441–465

Yang H, Rose N (2005) Trace element pollution records in some UK lake sediments, their history, influence factors and regional differences. Environ Int 31:63–75

Yang ZR, Grahan EY, Luons WB (2003) Geochemistry of Pyramidal Lake sediments: influence of anthropogenic activities and climatic variations within the basin. Environ Geol 43:688–697